Archives of Civil and Mechanical Engineering (2023) 23:34
https://doi.org/10.1007/s43452-022-00564-9

ORIGINAL ARTICLE

Theoretical and experimental analysis of guided wave propagation in plate-like structures with sinusoidal thickness variations

Beata Zima[1] · **Jochen Moll**[2]

Received: 28 July 2022 / Revised: 11 October 2022 / Accepted: 31 October 2022

Abstract
Guided waves have attracted significant attention for non-destructive testing (NDT) and structural health monitoring (SHM) due to their ability to travel relatively long distances without significant energy loss combined with their sensitivity to even small defects. Therefore, they are commonly used in damage detection and localization applications. The main idea of incorporating guided waves in NDT and SHM is based on processing the received signals and appropriate interpretation of their characteristics. A great amount of research devoted to diagnostics of plate-like structures considers specimens with constant thickness, which significantly facilities the diagnostic process. In such a case the velocity is also assumed to be constant. However, the developed diagnostic methods should be applicable, especially for the structures exposed to an aggressive environment, excessive load, or unfavorable weather conditions, etc., when the probability of damage occurring is much higher. In such cases, the assumption about the uniform thickness alongside the propagation path cannot be applied in every case. Thus, the present study is focused on wave propagation in metallic plates with variable thickness. The results of theoretical, numerical and experimental investigations of antisymmetric Lamb mode propagation in aluminum plates with a sine-shaped surface are presented. In the first step, the influence of non-uniform thickness distribution on wave velocity has been described. Next, the inverse problem aimed at shape reconstruction based on time of flight (ToF) analysis and spatially varying wave velocity was solved and compared with the standard dispersion curve-fitting method.

Keywords Guided waves · Irregular plate · Numerical simulations · Experimental tests · CNC manufacturing

1 Introduction

Guided wave propagation in metallic plates has been extensively studied in the last years, as they are a promising method for noninvasive diagnostics [1]. In particular, wave-based methods are commonly used because of their ability to travel long distances without significant amplitude reduction. Special attention has been paid to damage detection and localization procedures for plates [2]. In many cases, the faulty region is localized based on the time lags between reflections captured by transducers in the network. Based on the ToF and propagation velocity the possible localizations of the damage can be determined [3].

✉ Beata Zima
beata.zima@pg.edu.pl

[1] Faculty of Mechanical Engineering and Ship Technology, Gdańsk University of Technology, 80-233, Gdańsk, Poland

[2] Department of Physics, Goethe University Frankfurt, 60438 Frankfurt, Germany

The velocity of the guided wave can be established by solving the Rayleigh–Lamb equation and tracing the dispersion curves representing frequency–velocity relationships [4]. It is well-known that their shape strongly depends on material parameters and plate thickness. In the majority of so far developed algorithms, the assumption about the homogeneity, isotropy as well as constant thickness is usually applied, which significantly facilities the description of considered phenomena and the proposed algorithm of damage detection and localization [5]. Usually, such an assumption is justified, because the variability of material parameters and geometric imperfections of healthily metallic structures are negligible. However, the developed diagnostic methods should be applicable, especially for the structures exposed to an aggressive environment, excessive load, or unfavorable weather conditions, etc., when the probability of damage occurrence is much higher. In such cases, the assumption about the uniform thickness alongside the propagation path cannot be applied indiscriminately in every case. One example is general degradation caused by a corrosive environment. The

Published online: 19 November 2022

general corrosion degradation leads to non-uniform thickness reduction [6]. The incorrect assumption about constant wave velocity may lead to inaccuracies in damage detection and localization due to changes in the dispersion characteristics. Another example, which should be considered taking into account the non-uniform thickness are structures covered with ice [7]. The thickness of the additional ice layer changes periodically and depends on region, temperature, and season. The structures strengthened with additional adhesive layers [8], or even the skeletal elements [9] tested using elastic waves also require rejecting the assumption about constant thickness. Thus, the development of the NDT method for Structural Health Monitoring (SHM) forced the need of considering wave propagation in specimens with more complex geometry.

In the literature the problem of wave propagation in structures with non-uniform geometry has been considered by many researchers ([10–18]). The ultrasonic mode conversion phenomena under waveguide thickness variation employing the hybrid boundary element method was considered by Cho [10]. The influence of the local thickness of the waveguide and the slope of the tapered plate on the modal conversion was investigated by Predoi et al. [11]. The behavior of guided waves in specimens with Gaussian variation of their section, located between two areas of constant thickness was analyzed by Marical et al. [12]. The Lamb wave reflection and transmissions from a plate step discontinuity were numerically determined as a function of incident mode, excitation frequency, type of thickness variation, and waveguide shape. Pageneux and Maurel [13] dealt with the theoretical analysis of wave propagation in specimens with varying thickness. They rearranged the equations of elasticity to derive the new system of coupled-mode equations describing wave motion in specimens with a thickness described by the Gaussian function. The characteristics and the generation mechanism of the nonlinear symmetric Lamb mode propagating downslope in a plate with slowly linearly varying thickness were investigated by Hu et al. [14]. The phenomenon of mode conversion guided wave mode in plates with variable thickness was studied by El-Kettani et al. [15] and Nurmalia et al. [16]. Wave propagation in the tapered multilayered composite plate and the procedure of thickness variability determination using a combined method based on vibrometry and a terahertz time-domain system was described by Moll et al. [17]. In the next stage, the wave-based damage detection and localization technique, which considered the adiabatic wave motion was developed [18].

Despite enormous effort devoted to the detailed description of wave propagation phenomenon in specimens with complex geometry, the problem of thickness variability assessment based on a limited number of ultrasonic measurements has not been solved, yet. So far, mainly the dispersion-curve fitting was applied to determine the average thickness [19]. Because the dispersive relationship between thickness and velocity is not linear, the average velocity cannot be used to determine the average thickness and this method is suitable only for specimens with uniform thickness. To the authors' best knowledge the wave-based method of estimation of the thickness variability of non-uniform structures has not been presented, yet. Meanwhile, the aforementioned paper by Moll [18] undoubtedly proved that irregular geometry of the monitored structure has a great impact on the final results of the monitoring and diagnostic procedures (i.e., determined damage position).

The presented study is an essential prerequisite in the development of novel wave-based diagnostic methods applicable to structures characterized by complex shapes with non-uniform thickness. As mentioned, taking into account the possible thickness variability is crucial in the case of specimens subjected to general degradation. From the engineering point of view, estimation of the minimal plate thickness alongside the propagation path is more important than average plate thickness, because it determines the load capacity of the entire structure. In the case of ice accretion monitoring, the maximal thickness of an additional layer is searched. To this aim, plate shape reconstruction is required. The numerical and experimental tests were preceded by theoretical analysis focused on the influence of thickness variability on wave propagation velocity. Next, the inherent issues associated with solving the inverse problem aimed at shape reconstruction based on wave propagation signals have been discussed. The standard approach to determining the exact thickness distribution would require considering the underdetermined system of equations, which is an ill-posed problem [20]. Thus, the negligible changes in input data may produce large differences in the estimated thickness variability. In this study, the different approach allowing for avoiding typical difficulties associated with inverse problems has been presented which is an original element of the paper. The proposed method is based on assumption that any surface can be approximated by a certain function. Instead of determining the exact geometry of the plate, only several parameters of the function describing plate geometry have been estimated. Such formulation significantly reduces the number of unknowns and in consequence facilitated solving the problem of plate shape determination. The correctness of the conducted reasoning has been verified during experimental and numerical tests conducted on specially designed and prepared aluminum plates. Because the more complex thinning geometry is usually more complicated for analysis than tapered waveguides with abrupt thickness changes, the authors tested special plates prepared using computerized numerical control (CNC) manufacturing. Guided waves were propagated in four plates with a sinusoidal-shaped surface. The functions defining surface shape differed only in phase shift, which forced the thickness distribution

variability. On one hand, the smooth sine shape provided thickness variability and allowed for analysis of its influence on wave propagation velocity. On the other hand, it allowed for avoiding undesired effects related to localized stepped thickness changes. The additional advantage of considering the sine shape is the potential to transfer the idea to more complex structures. According to the Fourier theorem, each function can be expressed as a sum of varying sinusoidal components [21]. This study proves that it is possible to extract information about the parameters of a single sine component from the ToF of the guided wave, which allows concluding that also the geometry described by more complex functions containing several sine components can be reconstructed in this way.

The average velocity of fundamental antisymmetric A0 mode was used as an indicative parameter to evaluate the parameters defining plate geometry. One of the advantages of the proposed approach is the limited sensor network used. The theoretical analysis was conducted with the assumption that the wave is excited by a single actuator and received by a single sensor localized on both ends of the tested plates. This significantly facilities the diagnostic procedure and reduces the analysis time and the cost of the investigation. To demonstrate the advantages of the novel method, in the first step the most common approach based on dispersion curve fitting was used to determine average plate thickness. The errors obtained using the two aforementioned approaches differ significantly in favor of rejecting the assumption about constant thickness. The study involved experimental tests as well as the corresponding numerical simulations.

The paper is organized as follows. Section 2 contains a brief description of the influence of plate thickness variability on wave propagation velocity alongside the propagation path. Section 3 presents the materials and methods used during experimental and numerical analysis. Section 4 presents the results of solving the direct and inverse problem, while Sect. . 5 concludes the paper. The advantages, as well as the drawbacks and limitations of the proposed approach, are faithfully discussed.

2 Wave propagation in a plate with variable thickness

Wave propagation velocity in plates for particular wave modes can be easily predicted based on the dispersion curves which represent the solution of the well-known Rayleigh–Lamb dispersion equation [4]. However, this equation is valid only for plates with constant thickness, while plates characterized by non-uniform thickness require another approach. Let us consider the irregular plate, depicted in Fig. 1, divided into N divisions with a length Δl. The time needed to travel the distance Δl is equal to

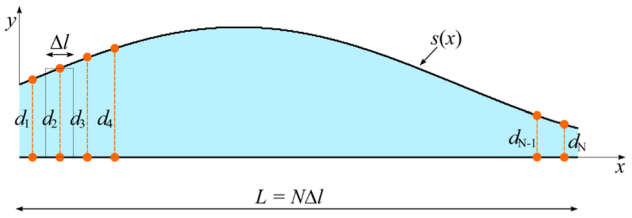

Fig. 1 Plate with variable thickness—explanation of the symbols used in the text

$$\Delta t_i = \frac{\Delta l_i}{c_{g_i}} \tag{1}$$

where c_{g_i} is the group velocity determined for thickness d_i. The total ToF along the distance L is a sum of the particular times of flight along with the distances Δl:

$$ToF = \sum_{i=1}^{N} t_i = \sum_{i=1}^{N} \frac{\Delta l}{c_{g_i}} = \Delta l \sum_{i=1}^{N} \frac{1}{c_{g_i}} \tag{2}$$

while the average velocity alongside the distance L is described as

$$c_{g,mean} = \frac{L}{ToF} = \frac{L}{\Delta l \sum_{i=1}^{n} \frac{1}{c_{g_i}}} = \frac{N}{\sum_{i=1}^{n} \frac{1}{c_{g_i}}} \tag{3}$$

Based on the above equations, one can conclude that the average wave velocity does not depend on the exact plate shape, but only on the thickness distribution, which in turn implies that the plate shape reconstruction cannot be realized using only wave velocity measured alongside the certain distance.

3 Experimental setup and data analysis

3.1 Plate shape design

In the following study, the plates with one surface flat and one surface described by sine function have been investigated (Fig. 2). On one hand, the smooth sine shape of the plate surface provided thickness variability and allowed for analysis of its influence on wave propagation velocity. On the other hand, it allowed for avoiding undesired effects related to abrupt thickness changes. In the plate with stepped thickness, the additional reflections triggered by geometry irregularities and mode conversions would be observed which would require a more complex interpretation. Moreover, the histogram describing plate thickness distribution is much simpler in the case of the plate with stepped thickness.

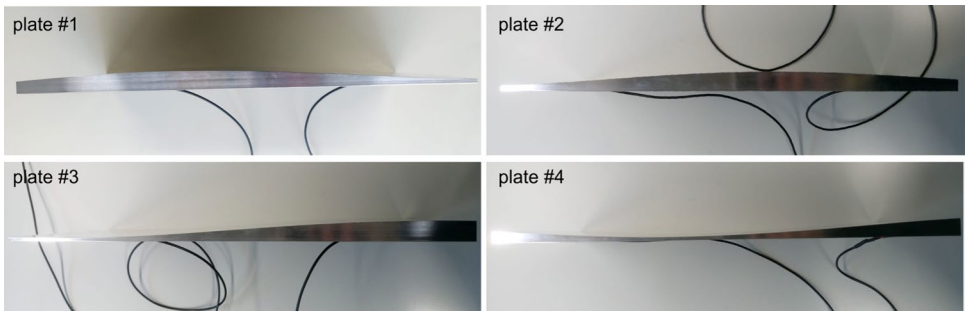

Fig. 2 Photos of investigated plates

The upper plate surface has been described by the following equation:

$$s(x) = A \cdot \sin(kx - \varphi) + h_0 \tag{4}$$

where A is the amplitude, k is the wavenumber, φ is the phase shift and h_0 is the initial plate thickness. All these parameters were established by taking into account the difference in wave velocity between particular plates as well as the technological possibilities, cost, and execution time of their manufacturing. We aimed to provide that the differences in the ToF will be observable while maintaining manufacturing safety. The procedure of plate shape optimization is discussed in the following section.

The plates were manufactured using a special CNC milling machine. Their total length L was 400 mm and width W was 250 mm and these dimensions were dictated by the size of the operating space. The thickness $h_0 = 10$ mm was the trade-off between the mass of the specimen (the manufacturing process was much safer and more efficient for specimens with higher mass) and the theoretically determined differences in ToF (the greater differences were noted for smaller thicknesses).

Four different plates differing in phase shift were considered in this study. The φ values were chosen by comparing the average velocity calculated according to Eq. (2) in plates differing in phase shift φ. Exemplary relationships between group velocities for 50 and 150 kHz and variable phase shift calculated for fixed parameters A and h_0 or k and h_0 are presented in Figs. 3 and 4, respectively. Based on the obtained results one can conclude that the relationship between wave velocity, geometric parameters of considered plates, and frequency is strongly nonlinear and difficult to predict. Maximizing the difference in wave velocity between tested plates for a certain frequency does not provide a high difference in velocity for the whole frequency range. Finally, we have decided to test plates characterized by phase shift $\varphi_1 = 0$ and $\varphi_4 = \pi$: in the first case, the plate is characterized by the convex shape, while in the second case, the plate is concave. It was expected that the significant difference between thickness distributions will result in a difference in propagation characteristics, which is additionally confirmed by the results presented in Figs. 3a and . Regardless of the

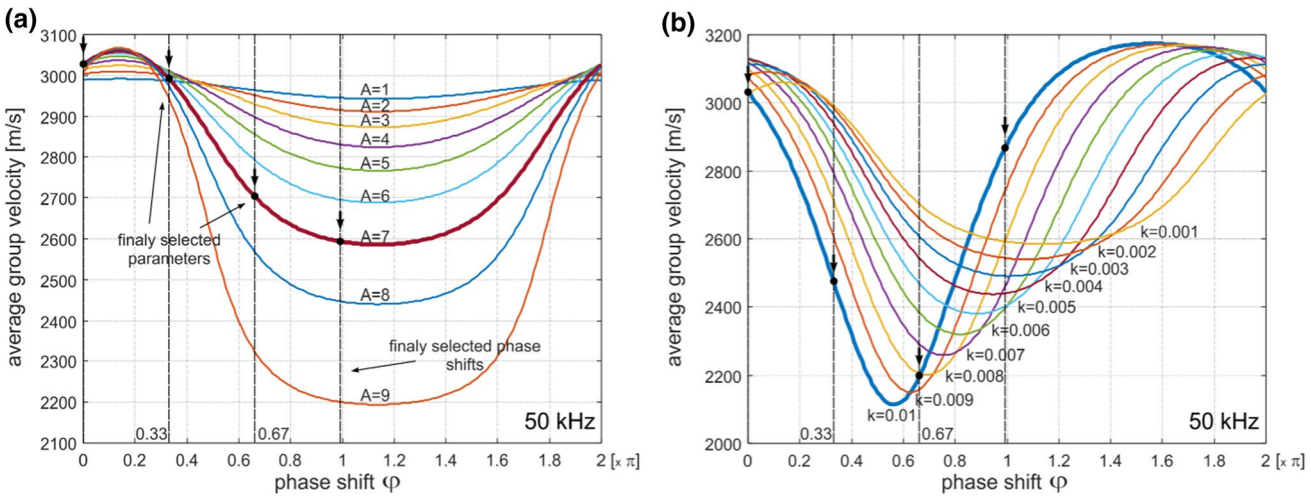

Fig. 3 Average group velocity for frequency of 50 kHz measured alongside the plate with surface described by Eq. (4) for a) fixed parameters $k = 0.01$ [rad/mm] and $h_o = 10$ [mm] and variable amplitude A and phase shift φ; b) fixed parameters $A = 7$ [mm] and $h_o = 10$ [mm] and variable wavenumber k and phase shift φ

value of amplitude A, the maximum difference in velocities (Fig. 3) was observed for plates characterized by phase shifts $\varphi = 0.13\pi$ and $\varphi = 1.13\pi$ for 50 kHz and by $\varphi = 0.27\pi$ and $\varphi = 0.82\pi$ for 150 kHz. In addition, two intermediate cases for $\varphi_2 = \pi/3$ and $\varphi_3 = 2\pi/3$ were investigated (Fig. 4).

To determine the remaining parameters, the average velocities for variables A and k for all plates have been calculated and depicted in the form of 3D graphs. Figure 5 depicts the exemplary results for 100 kHz; however, the observations made for other frequencies are similar. First of all, the differences in velocities for particular plates increase with increasing wave amplitude A. However, its upper limit was dictated by initial plate thickness h_0 and the manufacturing possibilities (the amplitude increase is associated with

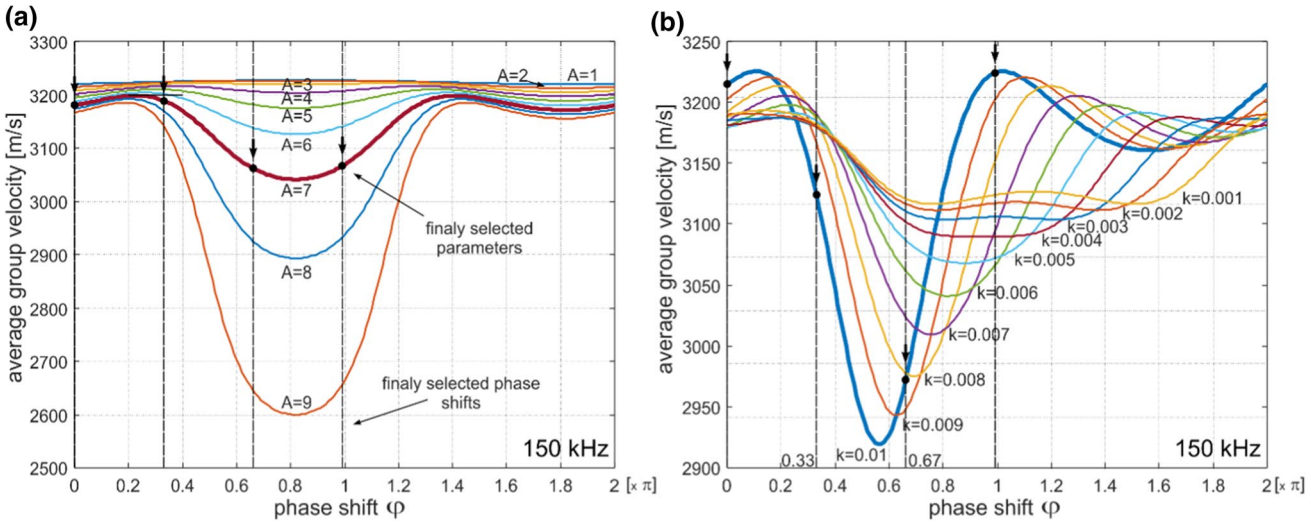

Fig. 4 Average group velocity for frequency of 150 kHz measured alongside the plate with surface described by Eq. (4) for **a** fixed parameters $k = 0.01$ [rad/mm] and $h_o = 10$ [mm] and variable amplitude A and phase shift φ; **b** fixed parameters $A = 7$ [mm] and $h_o = 10$ [mm] and variable wavenumber k and phase shift φ

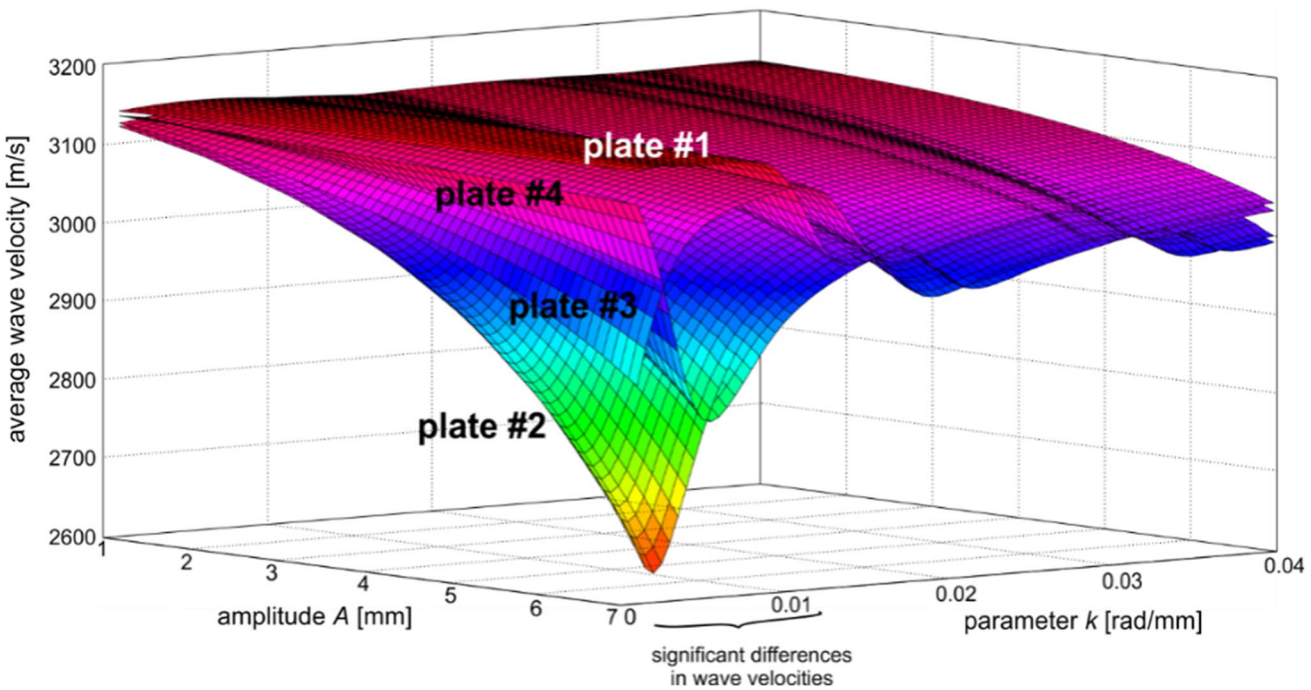

Fig. 5 Average group velocity alongside the plate with surface described by Eq. (4) for variable amplitude A and wavenumber k and for selected phase shifts (plate #1: $\varphi = 0$ [rad], plate #2: $\varphi = 1/3\pi$ [rad], plate #3: $\varphi = 2/3\pi$ [rad] and plate #4: $\varphi = \pi$ [rad])

the decrease of the thickness in the thinnest cross section, which must be greater than the certain minimal value to maintain manufacturing safety).

In the case of parameter k, the greatest differences in velocities were noted for its lower range $k \in < 0.001, 0.01 >$ [rad/mm]. If the wavenumber is higher and the number of cycles along the plate is greater and the differences in thickness distributions between the plates become less observable. The differences in velocities are particularly visible for very small values of the parameter k ($k = 0.001, 0.002$ [rad/mm]). However, for such a small wavenumber (i.e., $k = 0.001$ rad/mm) and long wavelength, the plates were more like plates with linearly variable thickness. To maintain the clear and more complex sine plate shape, a higher value of k was set. Finally, the function describing the upper plate surface has taken the following form:

$$s(x) = 7 \cdot \sin(0.01x - \varphi) + 10\,[\text{mm}] \tag{5}$$

The plates' geometry and histograms depicting thickness distributions are presented in Fig. 6. The histograms were performed for thickness measurements made with a step of 10^{-3} mm and the obtained values were grouped into 100 bins. The vertical axis of the histogram indicates the frequency of occurrence of the cross section characterized by a certain thickness.

3.2 Numerical modeling

Numerical plate models were developed using the commercial software Abaqus. For accurate modeling of mechanical guided wave propagation, the module Dynamic/Explicit was incorporated in this study. Three-dimensional models were built of eight-node brick elements with reduced integration (C3D8R). The transient wave propagation problem was solved with an integration step of 10^{-7} s, which was established by taking into account the Courant–Friedrichs–Lewy condition. To establish the finite element size, the simulations were preceded by a convergence study. The size of the elements did not exceed 1 mm^3. The excitation was applied as a time-dependent pressure applied on the area corresponding to the area of the real piezo transducers. The numerical model with applied pressure is presented in Fig. 7. The excitation function was in form of a five-cycle sine modulated by the Hann window:

$$p(t) = \begin{cases} 0.5p_0 \sin\left(2\pi ft\left(1 - \cos\left(\frac{2\pi ft}{n_w}\right)\right)\right) & t \in [0, T_w] \\ 0 & t \geq T_w \end{cases} \tag{6}$$

where f denotes the excitation frequency, p_0 is the excitation amplitude, T_w is the Hann window length and n_w is the number of time steps. Material parameters adopted in the model were as follows: elastic modulus $E = 70$ GPa, Poisson's ratio $v = 0.33$ and density $\rho = 2700$ kg/m^3.

The numerical simulations were performed for the 3D model, as the plain strain model would not provide the possibility to apply the excitation of the area corresponding to the actuator. Moreover, in the case of the 3D model, the reflections from boundaries present in experimental tests can be registered. Thus, the 3D model better reflects the actual experimental model. The accuracy of the numerical simulations has been proved by comparing the numerical results with experimental signals. The comparison is given in the further part of the paper.

3.3 Experimental setup

Guided waves were actuated and sensed by rectangular piezoceramic transducers with dimensions of 30×5 mm manufactured by Physik Instrumente. Using such kinds of transducers provides excitation of a straight wavefront, which in turn results in smaller inaccuracies in the ToF determination caused by imperfect transducers attachment.

The detail of the transducer attached to the plate surface is presented in Fig. 8a. To avoid non-perpendicular excitation, the transducers were glued to the flat surface. The signals were generated and registered by oscilloscope and function generator Handyscope HS5 (TiePie Engineering). To improve the signal-to-noise ratio, the receiver was connected to the high voltage amplifier PD200 (PiezoDrive Ltd, Shortland, NSW 2307, Australia), which transferred signals to a specially designed custom device Rammsbone described in detail in [22] (Fig. 8b). The excitation $p(t)$ was defined as a five-cycle sine modulated by the Hann window. The measurements were made for frequencies from 150 to 300 kHz with a step of 10 kHz. In total 16 carriers were used.

3.4 Data analysis

Recorded signals were processed in a MATLAB environment to extract the ToF for particular frequencies and to compare the velocities in various plates. The ToF was calculated using cross-correlation of the received signal and the excitation function [23].

In the first step, we have considered the direct problem. The influence of plate geometry on wave propagation velocity has been investigated by comparing the numerical and experimental signals, as well as the values of the ToF for particular plates and frequencies (Sect. 4.1). In the next step, we attempted to solve the inverse problem aiming to determine the plate shape using wave propagation velocity as an indicative parameter (Sect. 4.2).

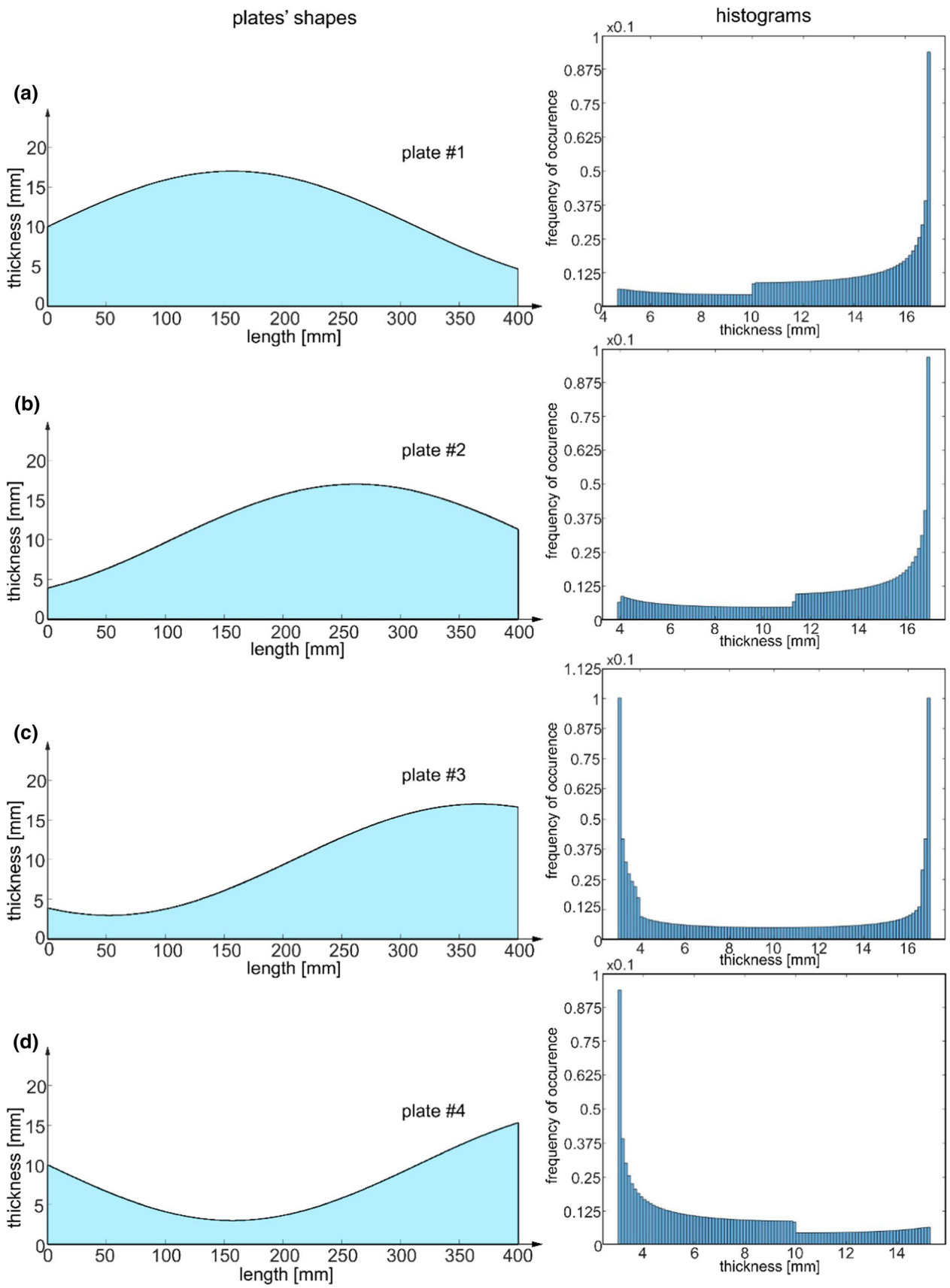

Fig. 6 Geometry of analyzed plates and histograms depicting thickness distributions: **a** plate #1, **b** plate #2, **c** plate #3 and **d** plate #4

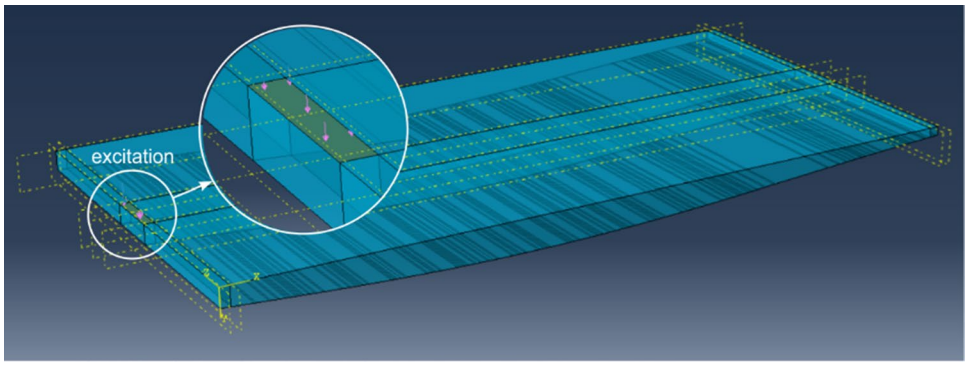

Fig. 7 Numerical model of plate#1 with applied pressure on the area corresponding to the area of the real transducers

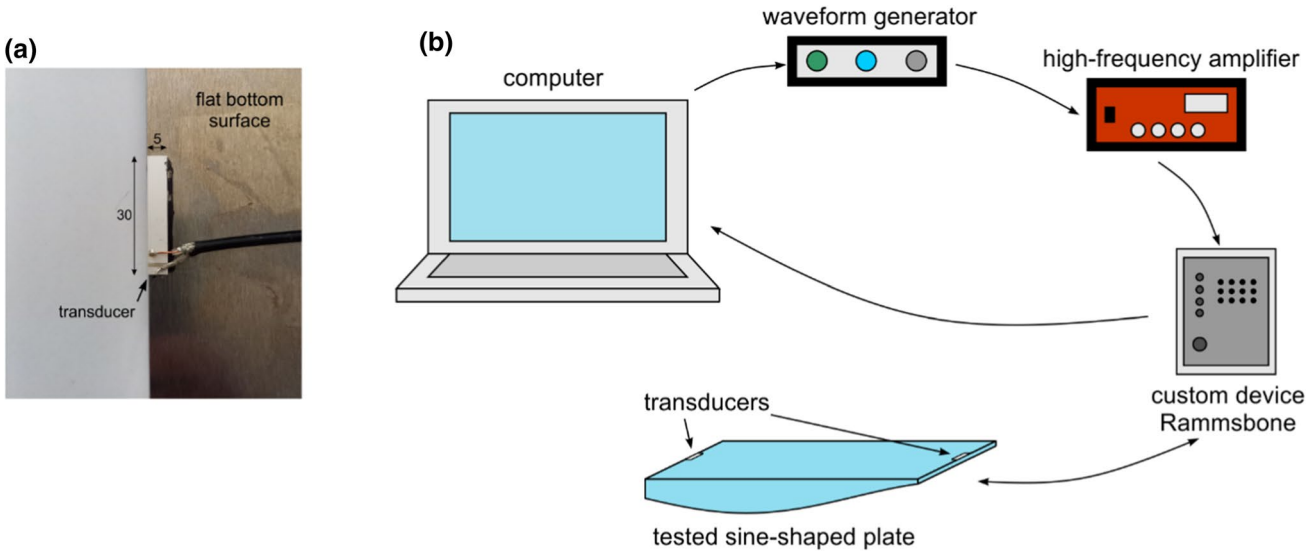

Fig. 8 Experimental investigation: **a** the detail of the rectangular transducer attached to the plate surface and **b** the scheme of an experimental setup

4 Results

4.1 Dispersion curves and mode conversion analysis

Signal processing and results analysis were preceded by considering dispersion curves and wave mode conversion phenomenon. Alongside the propagation path, the value of the frequency–thickness product changes, and as it exceeds the cutoffs of higher order guided modes, new wave modes can be triggered. Because particular modes differ in velocity, which is a crucial parameter used in plate shape reconstruction procedure, it is necessary to assess which modes can be excited in tested plates.

Figure 9 presents dispersion curves for aluminum plate, while Figs. 10 and depict the mode conversions phenomenon in two considered plates: convex plate #1 and concave plate #4, which are also two extreme cases in this study.

For comparison, the analysis of mode conversion was made for the maximal and minimal frequency used in the experimental investigation ($f_{\min} = 100$ and $f_{\max} = 300$ kHz). To indicate the cross sections, where mode conversion may occur, in the first step the function describing plate shape $s(x)$ defined by Eq. (5) was multiplied by considered frequency ($f_{\min}$ or $f_{\max}$). The frequency–thickness product $s(x) \cdot f$ was plotted by the black, solid line and compared with dispersion curves plotted with dashed lines. Such comparison allows for indicating places, where the frequency–thickness product exceeds the cutoffs of particular wave modes. These places were marked with dots and the regions characterized by a various number of possible wave modes were marked with different colors. Exemplary, in Fig. 10a, the results for plate #1, frequency 300 kHz and antisymmetric modes are presented. It can be seen that at the beginning (at the distance from 0 to 93 mm) two wave modes can be excited (A0 and A1). In the middle part, where the plate thickness increases

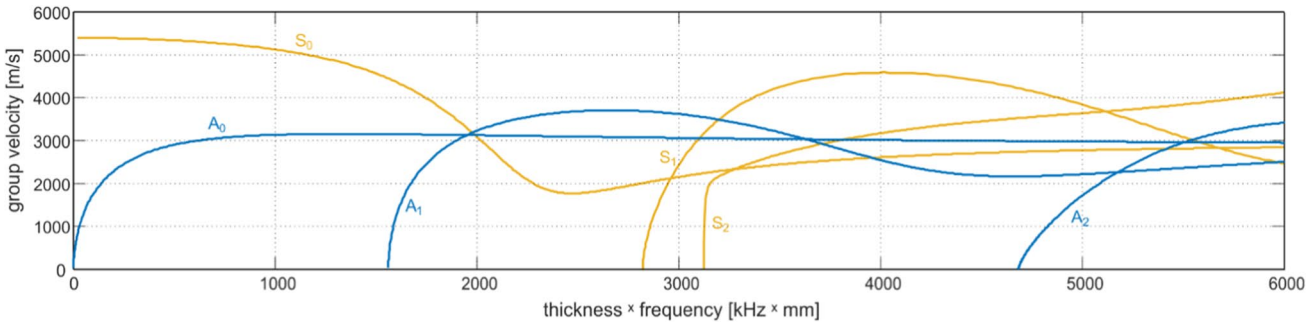

Fig. 9 Dispersion curves for aluminum plate ($E = 70$ GPa, $\nu = 0.33$ and $\rho = 2700$ kg/m.^{3})

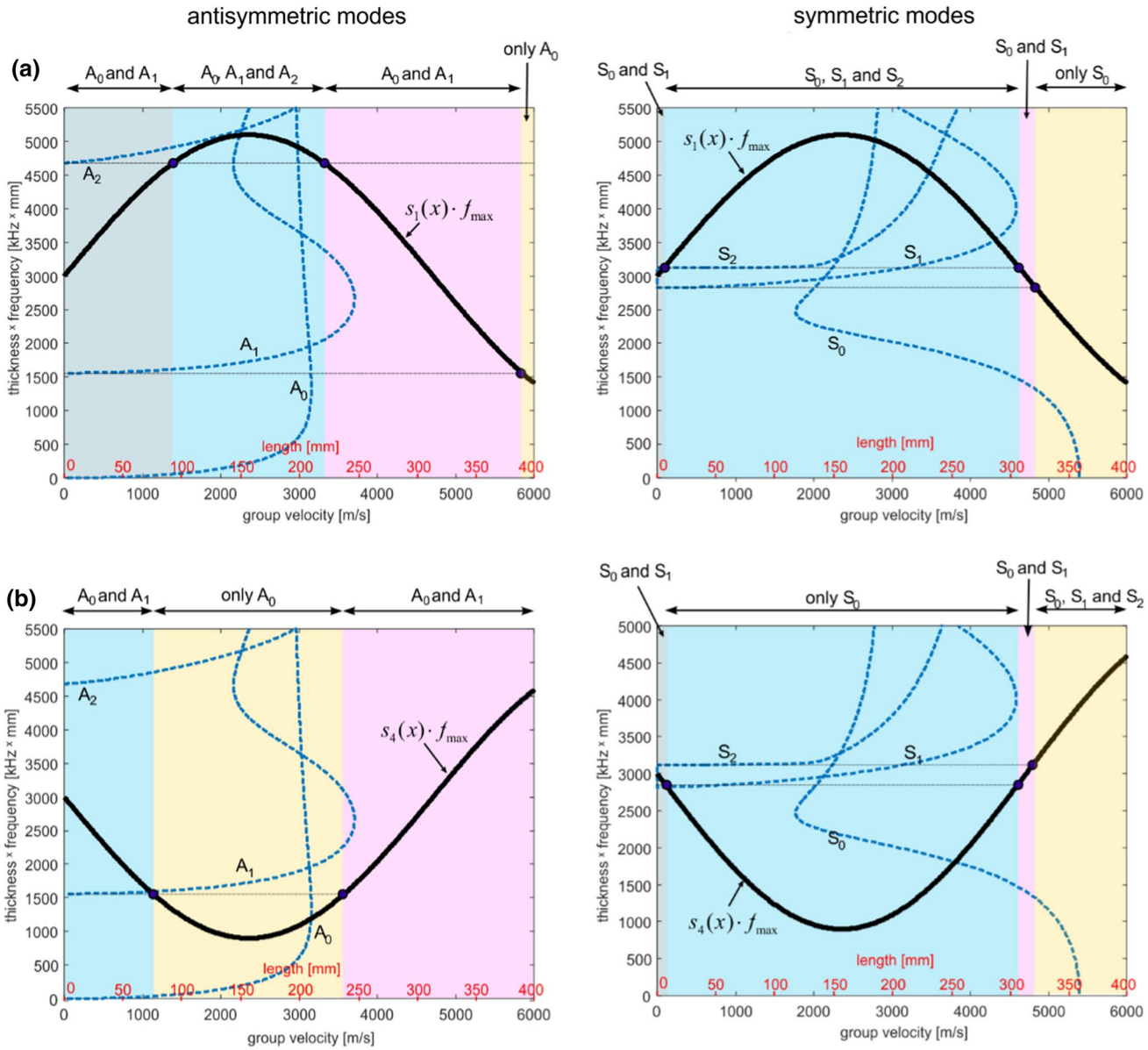

Fig. 10 Determination of wave modes which can occur in **a** plate #1 and **b** plate #4 for excitation frequency of 300 kHz

(93 mm to 221 mm), additionally, A2 mode may occur. However, when the plate thickness decreases it decays (221 mm to 390 mm) and finally, at the end of the plate only A0 may propagate (390 mm to 400 mm). As mentioned, the frequency of 300 kHz is the highest frequency used here, so the phenomenon is also the most complex for this case. Figure 11 presents the corresponding results for frequency $f_{\min} = 100$ kHz. For this frequency, the phenomenon is less complex and mode conversions almost do not occur.

The phenomenon of evanescence and reflection of higher order modes in places, where wave mode cutoffs are higher than plate frequency–thickness product has been described in detail in [15] and [16]. As the thickness is decreasing the higher order modes are reflected and propagate back along the plate or are converted into another lower order mode. Because the procedure of mode conversion analysis was performed for all plates and in each case, only S0 and A0 modes are the only modes, which may propagate alongside the entire plates lengths, further analysis is focused mainly on these fundamental modes.

4.2 The influence of plate thickness variability on wave velocity

The comparison of experimental and numerical signals for three chosen frequencies (100, 150 and 200 kHz) is presented in Fig. 12. The beginnings of arriving incident waves are zoomed in the figure to demonstrate the order in which waves are registered by the sensor. The time course of the incident wave can be the result of interference of both symmetric and antisymmetric modes. However, the theoretical

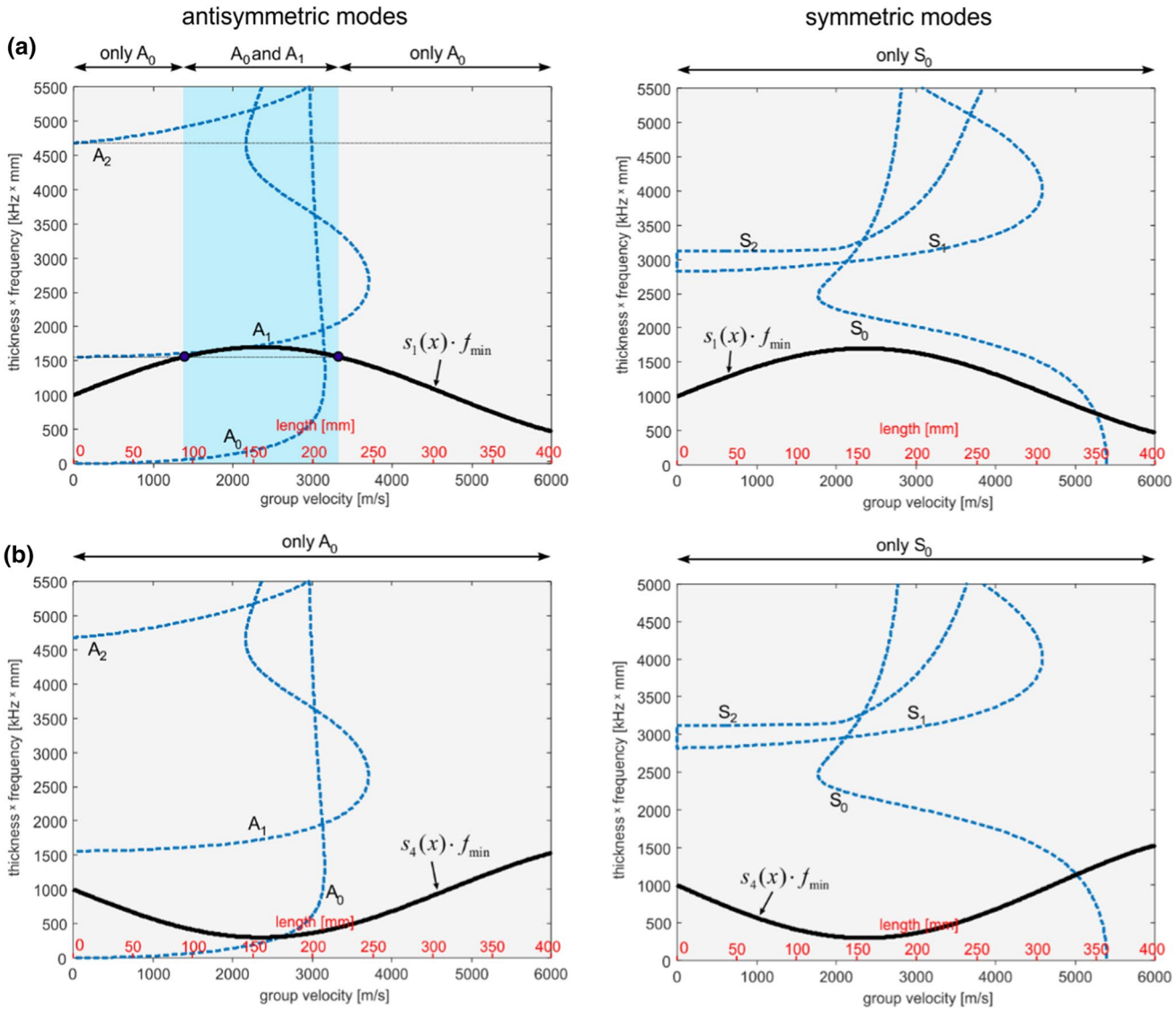

Fig. 11 Determination of wave modes, which can occur in **a** plate #1 and **b** plate #4 for excitation frequency of 100 kHz

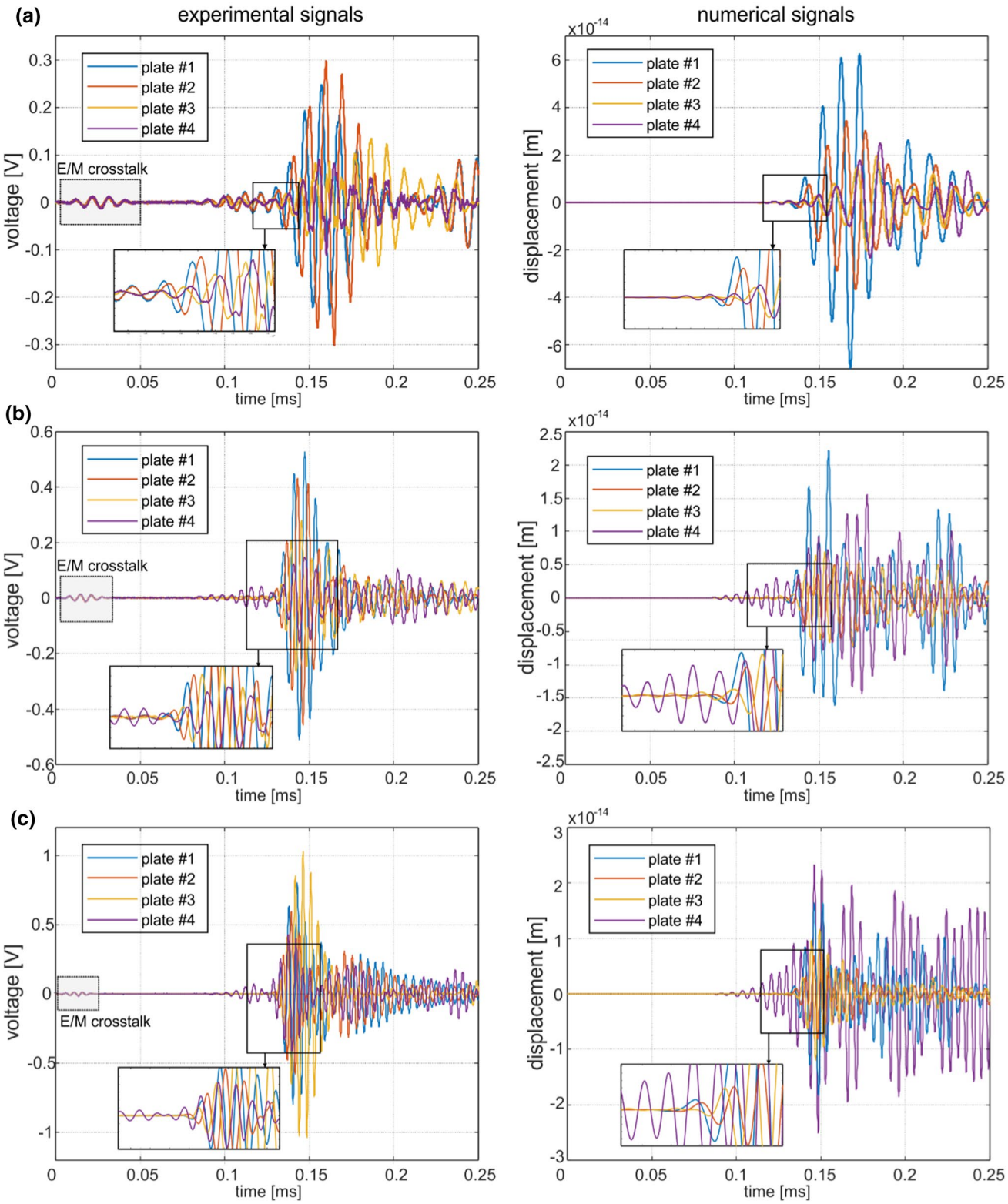

Fig. 12 Wave propagation signals obtained **a** experimentally and **b** numerically for exemplary frequencies of 100, 150 and 200 kHz

reasoning presented in Sect. 2 is valid for all modes' types. In every case, the consistency of the results is clearly visible and the order is the same for both experimental and numerical plates, which confirms the correctness of the statement about non-constant wave velocity in plates with non-uniform thickness. The relations between the amplitudes cannot be considered here, because it was strongly influenced during experimental tests by transducers attachment. Non-perfect transducers mounting together with non-uniform plate thickness alongside propagation path caused triggering symmetric S0 modes arriving before high-amplitude antisymmetric A0 mode. They are especially visible in plate #4, also in the case of numerical simulations. In experimental signals, the low-amplitude wave packet, which is E/M crosstalk has been identified and highlighted.

Figure 13 presents the experimentally, theoretically and numerically determined times of flight for investigated plates in the considered frequency range. In the case of the two first convex plates #1 and #2 ToF—frequency trend is upward. In the case of plate #3, which is a mixed convex–concave case, and concave plate #4 the downward trend is observed. Despite some discrepancies between the values, the trend is similar in each case. The differences in the ToF may result from inaccuracies in material parameters determination as well as from geometric imperfections. Moreover, the Lamb dispersion equations are derived for the two-dimensional plane strain plate model. In the real case, the primary emitted waves mix with their reflections from side edges which may result in complex wave patterns and consequence hinders signal interpretation. In addition, also symmetric modes are triggered and overlap with antisymmetric modes.

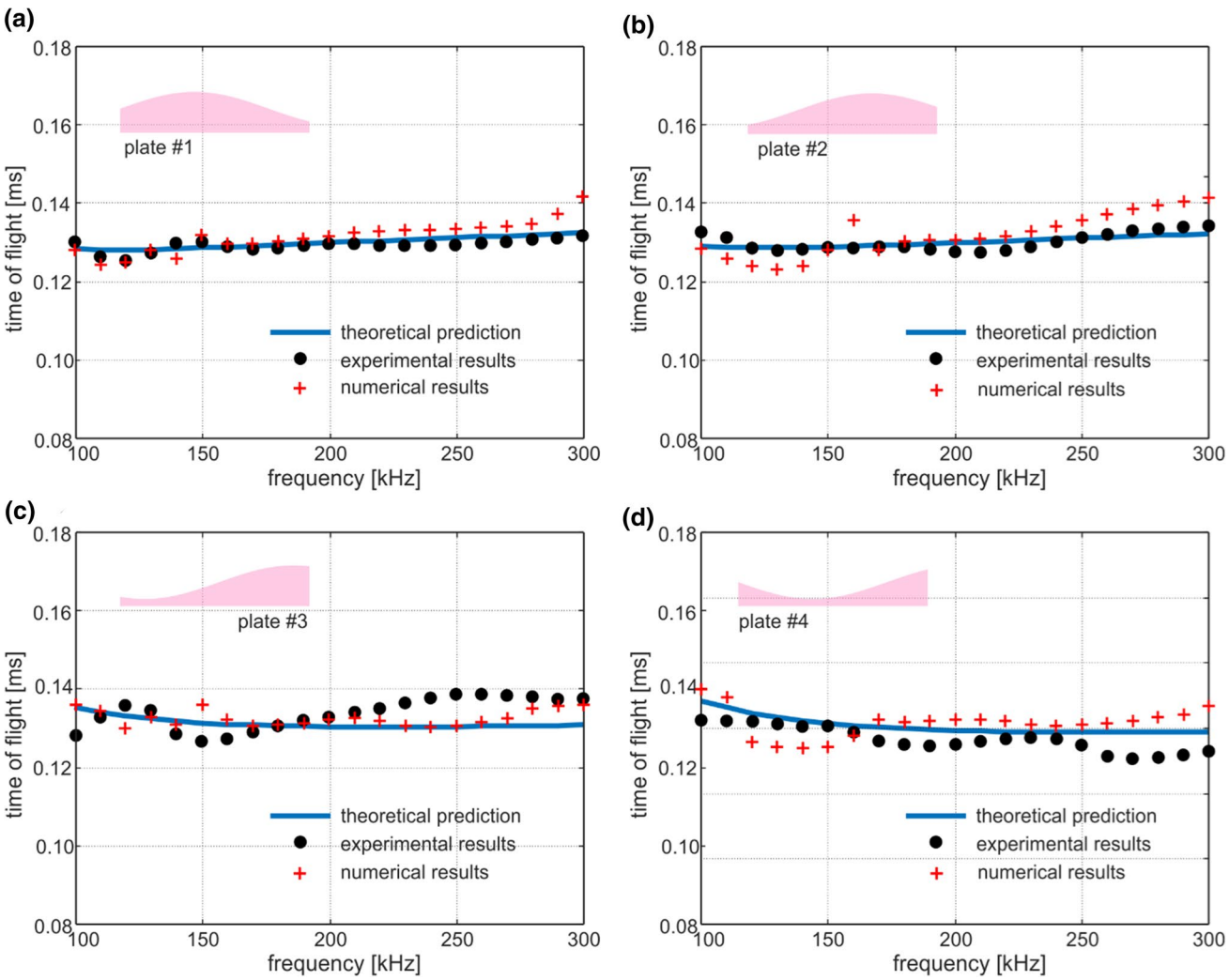

Fig. 13 ToF of antisymmetric A0 mode for varying excitation frequency in: **a** plate #1, **b** plate #2, **c** plate #3 and **d** plate #4

4.3 Solving the inverse problem—plate shape determination

The next step of the investigation is to solve the inverse problem intending to determine the specimen shape based on wave propagation velocity. It must be mentioned here that the exact shape determination based only on average wave velocity alongside propagation path is not possible because the velocity is dependent only on thickness distribution. It means that wave velocity in two different plates but with the same thickness, the distribution would be the same. To indicate the possible difficulties related to this task, the following relation should be considered:

$$\Psi x = t \tag{7}$$

In the above equation, the matrix Ψ is a kind of dictionary containing the reciprocals of wave propagation velocities for incorporated frequencies and various thicknesses. Vector x contains the information about the distances characterized by certain thickness, while the outcome is vector t containing the measured times of flight. The length of the vector t is determined by the number of measurements (number of signals received for different frequencies). To take into account the possible inaccuracies in ToF determination, Eq. (7) can be reformulated as follows:

$$\|\Psi x - t\|_{\infty} \leq \varepsilon \tag{8}$$

where ε is the level of inaccuracy. Unfortunately, for accurate determination of thickness distribution, the unknown vector x usually must contain a much greater number of elements than vector t, which in turn means that the solution of this problem requires solving an underdetermined system of linear equations. The optimal solution might be found by searching the highest of the lowest value of the appropriately defined objective function.

In this study, we present a different approach. Instead of searching for an optimal shape defined by a thickness histogram, which would be associated with a large number of unknown elements in x, the assumption that any surface can be approximated by a certain function has been applied. Instead of determining the exact histogram describing plate thickness distribution, only several parameters defining this function have been optimized. The results for two different cases differ in a number of unknown parameters defining the plate shape are presented. In the first stage, we assumed that the information about the sine shape of the plate surface and the parameter h_0 is available, while the amplitude A and phase shift φ are unknown. Such an approach is justified by practical aspects. First of all, we can assume that the shape of the monitored structure can be approximated by a certain function type. The structural object subjected to general, i.e., corrosion degradation is characterized by a more or less non-uniform shape ([6, 19]), which can be approximated by the sine/cosine function (Fig. 14).

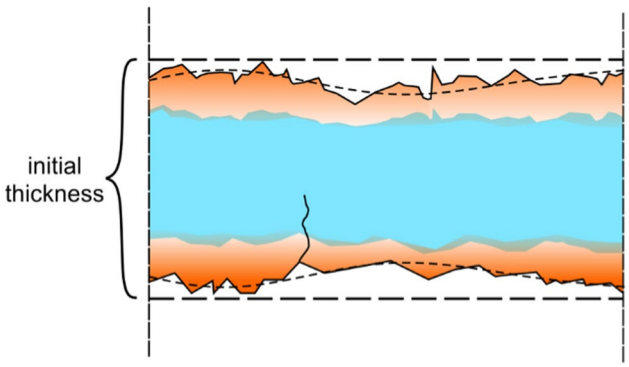

Fig. 14 Irregular surface of the specimen subjected to corrosion degradation

A similar case takes place in ice formation and its accretion monitoring [7]. The initial thickness of the monitored structure is usually known to the investigator. These assumptions significantly facilitate solving the inverse problem, which can be formulated as follows:

$$\min\left(\sum_{i=1}^{j}\left|t_t(A,\varphi,f_i)-t_e(f_i)\right|^2\right) \tag{9}$$

where t_t denotes the theoretical ToF for frequency f determined for plate defined by parameters A and φ, while t_e is experimentally determined ToF.

In the next stage, the difficulty level of the considered inverse problem increased and it was assumed that any parameter defining plate surface was known, i.e., the amplitude, wavenumber, initial thickness, and phase shift. The such analysis allowed to assess the effectiveness of shape reconstruction depending on the number of unknowns.

As mentioned above the experimentally determined ToF t_e differ from theoretical results t_t mainly because of geometric and material imperfections. However, the method of the ToF determination has also an impact on the final results [23]. To eliminate the systematic errors related to the adopted methodology, the minimal sum of residuals was calculated as the squared difference between the theoretical and measured derivatives of the t_t and t_e was searched:

$$S_i = \frac{d}{df}t_t(A,\varphi,k,h_0,f_i) - \frac{d}{df}t_e(f_i)$$
$$\min\sum_{i=1}^{n} S_i^2 \tag{10}$$

Such formulation of the problem allows for considering not the exact values but the relation between the ToF obtained for particular frequencies.

It should be mentioned here that the zero amplitude entails uniform plate thickness, while the plates with linearly varying thickness can be approximated by a sine function with a low k value. Thus, the assumption about sinusoidal plate shape does not exclude the estimation of the thickness distribution of specimens characterized by less complex shapes. The solution of inverse problems was additionally preceded by determining the average plate thickness using a well-known approach based on fitting the theoretical dispersion curves, which was compared with exact and reconstructed thicknesses in the further part of the paper.

4.3.1 Stage I: solving the inverse problem under the assumption of constant plate thickness

The method of rough plate shape evaluation based on wave velocity has been widely analyzed in literature [19]. It is based on fitting the theoretical dispersion curve to the experimental velocities. The main assumption in this approach is that the average wave velocity can be used to determine the average plate thickness h_a, while the possible variability of the geometric parameters is omitted. As mentioned, it may lead to an overestimation of the actual minimal thickness $h_{\min}$, which is critical for the state of the entire structure. Therefore, for the level of thickness overestimation assessment, solving the inverse problem has been preceded by determining the average plate thickness by dispersion curve fitting (Table 1). In each case (Tables 3, 5 and 7), the average plate thickness was compared with the minimum and maximum plate thickness $h^r_{\min}$ obtained from the reconstructed plate shape.

To determine the average plate thickness h_a, the minimal value of the following function was searched:

$$\frac{1}{j}\sum_{i=1}^{j}\left(c_g^{t,i}(h)-c_g^{i}\right)^2 \tag{11}$$

where j is the number of measured signals (frequencies), c_g^t and c_g^i is theoretical and experimental or numerical group velocity, respectively. The average thicknesses obtained for each plate based on experimental and numerical velocities are summarized in Table 1. In addition, the average thickness calculated as

$$h_a=\frac{\int_0^L s(x)dx}{L} \tag{12}$$

was added for comparison. The differences between experimental h_a^e and numerical h_a^n average thicknesses are the result of outliers observed for lower frequencies (up to 160 kHz). For lower frequencies, the symmetric mode propagates faster than the antisymmetric mode. Due to mode conversion caused by irregular geometry, the symmetric mode is clearly visible in numerical signals and because of the relatively short propagation path, both modes A0 and S0 interfere with each other. In consequence, the ToF for lower frequencies is characterized by significant inaccuracy, which in turn influences the average plate thickness determined by tracing and fitting dispersion curves. For higher frequencies A0 mode propagates faster than S0 mode, so the first peak is attributed to the antisymmetric mode which is considered here and the ToFs are characterized by higher agreement with theoretical predictions (see Fig. 13).

Nevertheless, in three cases (plates #1, #2 and #4) the average plate thickness h_a calculated based on the plate cross-sectional area [Eq. (12)] coincides well with experimentally determined average thicknesses. These findings suggest that the dispersion curve fitting can be potentially used as an additional step in the exact plate shape reconstruction procedure presented in the next section. The average plate thickness determined for reconstructed shape according to Eq. (12) may be compared with the results of dispersion curve fitting.

4.3.2 Stage II: plate shape determination for two parameters unknown (amplitude, phase shift)

In the second stage, Eq. (10) was solved for pre-assumed initial thickness h_0 and wavenumber k. The minimum value of S was searched for phase shift varying from 0 to 2π with a step of 0.01π, while the amplitude varied from 0 to 9 mm with a step of 1 mm. The upper limit of the amplitude was determined based on the initial plate thickness. The amplitude cannot be greater than plate thickness, because it would entail zero or negative thickness, which has no physical sense.

Table 1 Comparison of experimental and numerical average plate thicknesses determined based on fitted dispersion curves of A0 mode and average thickness of investigated plates calculated according to Eq. (12)

Specimen	Experimental average plate thickness h_a^e [mm]	Numerical average plate thickness h_a^n [mm]	Average plate thickness h_a [mm]
Plate #1	11.700	25.200	12.900
Plate #2	13.100	29.500	12.600
Plate #3	24.100	40.000	9.700
Plate #4	5.600	34.500	7.100

First, the possibility of plate shape reconstruction has been verified numerically. The reconstructed plates' shapes compared with exact plates are presented in Fig. 15, while the comparison of the parameters A_n and φ_n with the real values A and φ is summarized in Table 2.

The quality of the reconstruction is high which proves the correctness of the conducted reasoning. In every case, the shape type (concave or convex) has been recognized correctly. The amplitude was slightly overestimated but ΔA did not exceed 2 mm, while the greatest difference in determined and exact phase shift was noted for plate #4 and was equal to 0.2π. The discrepancies between numerically obtained shapes and the exact plates' shapes can be attributed to the mixing of primary waves with their reflections as well as the triggered symmetric modes, which caused the difficulties in extracting the correct wave packet and influenced the time course of registered signals.

Table 3 contains the comparative analysis of minimal and maximal thickness extracted from reconstructed shapes and average thickness obtained from dispersion curve fitting h_a with exact plate shape ($h_{\min}$, $h_{\max}$). The relative errors were also calculated for minimal and maximal thickness from the reconstructed shape $h^r_{\min}$ and $h^r_{\max}$:

$$\Delta_r^{\min} = \left|\frac{h_{\min} - h^r_{\min}}{h_{\min}}\right| \cdot 100\% \ , \ldots \Delta_r^{\max} = \left|\frac{h_{\max} - h^r_{\max}}{h_{\max}}\right| \cdot 100\% \tag{12}$$

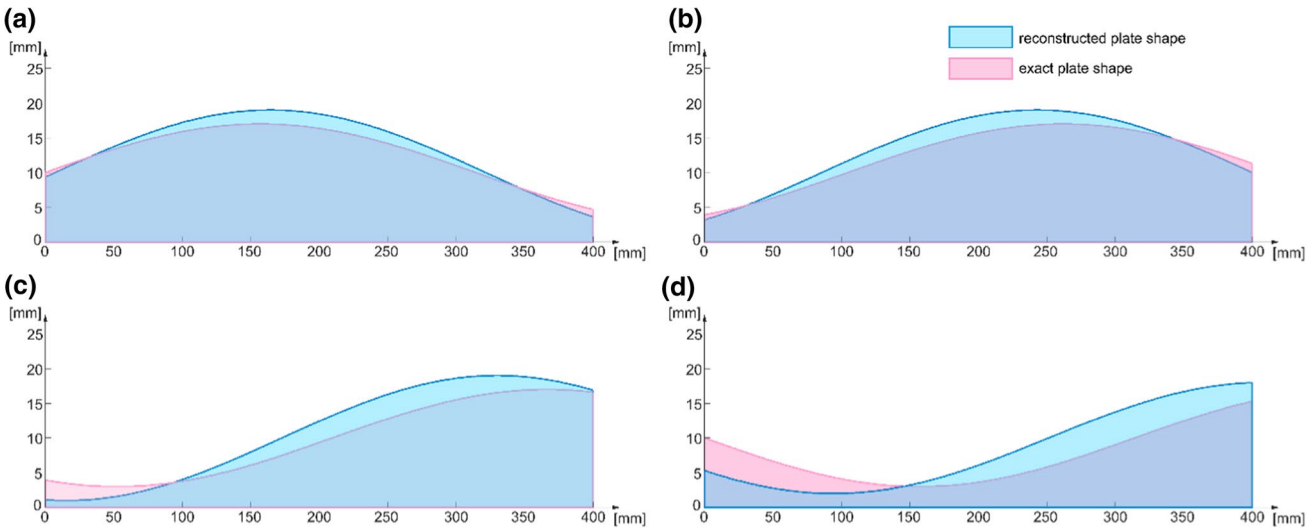

Fig. 15 Results of the numerical investigation aimed to determine the shape of the plate with non-constant thickness: the comparison of exact plate shapes with determined based on the numerical ToF measurements for **a** plate#1, **b** plate#2, **c** plate#3 and **d** plate#4

Table 2 Comparison of exact and numerically determined amplitude and phase shift describing the sine-shaped plate surface

	Parameters defining sine function					
	A [mm]	A_n [mm]	$\Delta A = \lvert A - A_n \rvert$	φ	φ_n	$\Delta\varphi = \lvert\varphi - \varphi_n\rvert$
Plate #1	7	9	2	0	0.024π	0.024π
Plate #2	7	9	2	0.33π	0.274π	0.056π
Plate #3	7	9	2	0.67π	0.55π	0.12π
Plate #4	7	8	1	π	0.8π	0.2π

Table 3 Comparison of the minimum and maximum thickness of numerically reconstructed plate, average thickness determined based on the ToF, with actual plate thickness

	Actual minimum thickness h_{min}	Actual maximum thickness h_{max}	$h^r_{\min}$ [mm]	$h^r_{\max}$ [mm]	$\Delta_r^{\min}$ [%]	$\Delta_r^{\max}$ [%]	h^n_a [mm]	$\Delta_a^{\min}$[%]	$\Delta_a^{\max}$[%]
Plate #1	4.702	17	3.70	19	21.32	11.76	25.20	435.94	48.24
Plate #2	3.938	17	3.20	19	18.74	11.76	29.50	649.11	73.53
Plate #3	3.000	17	1.00	19	66.67	11.76	40.00	123.33	135.29
Plate #4	3.000	15.3	2.00	18	33	17.65	34.50	105.00	125.49

and for average thickness from dispersion curve fitting h_a:

$$\Delta_a^{\min} = \left|\frac{h_{\min} - h_a}{h_{\min}}\right| \cdot 100\%, \ldots \Delta_a^{\max} = \left|\frac{h_{\max} - h_a}{h_{\max}}\right| \cdot 100\% \tag{13}$$

The maximum errors were highlighted. In almost every case the simplified and incorrect assumption about constant plate thickness when the averaged thickness was compared with actual plate dimensions ($\Delta_a^{\min}$ and $\Delta_a^{\max}$) resulted in a maximum error. The assumption about uniform thickness and constant velocity has led to a significant overestimation of minimum thickness, as well as the underestimation of the maximum thickness. The value $\Delta_a^{\min}$ reached over 649%. From the engineering point of view, such significant thickness overestimation is a particularly unfavorable and dangerous situation, because it may result in a substantial overestimation of structural load capacity. One can conclude that the assumption about constant thickness in the case of the specimen with non-uniform thickness always leads to significant thickness over- or underestimation or both.

Estimation of the minimum and maximum thickness based on the reconstructed shape resulted in much lower errors, which demonstrates the utility of the proposed approach. The highest error was noted for plate #3 when the minimum thickness was additionally underestimated. Despite the significant error value, this case clearly indicates an important advantage of the developed approach to plate shape reconstruction. An assumption about non-constant plate thickness has led to overestimation of maximum thickness and underestimation of minimum thickness, while the situation was exactly the opposite if the thickness was assumed to be constant. If the non-uniform plate shape was considered, even in the case of some inaccuracies in shape reconstruction, we were still on the safe side.

In the next step the experimental data were processed in the same way and the reconstructed plate shapes' are given in Fig. 16, while Table 4 contains the values of the calculated amplitudes and phase shifts. In three cases the amplitude was overestimated by 2 mm, while the thickness of plate#4 was underestimated by 4 mm. The maximal difference between exact and estimated phase shift φ was noted for plates #1 and #4 and was equal to 0.16π and 0.15π, respectively. In total, the lowest quality of shape reconstruction obtained for plate #4 is also visible in the figure, but still, the clear concave shape has been detected.

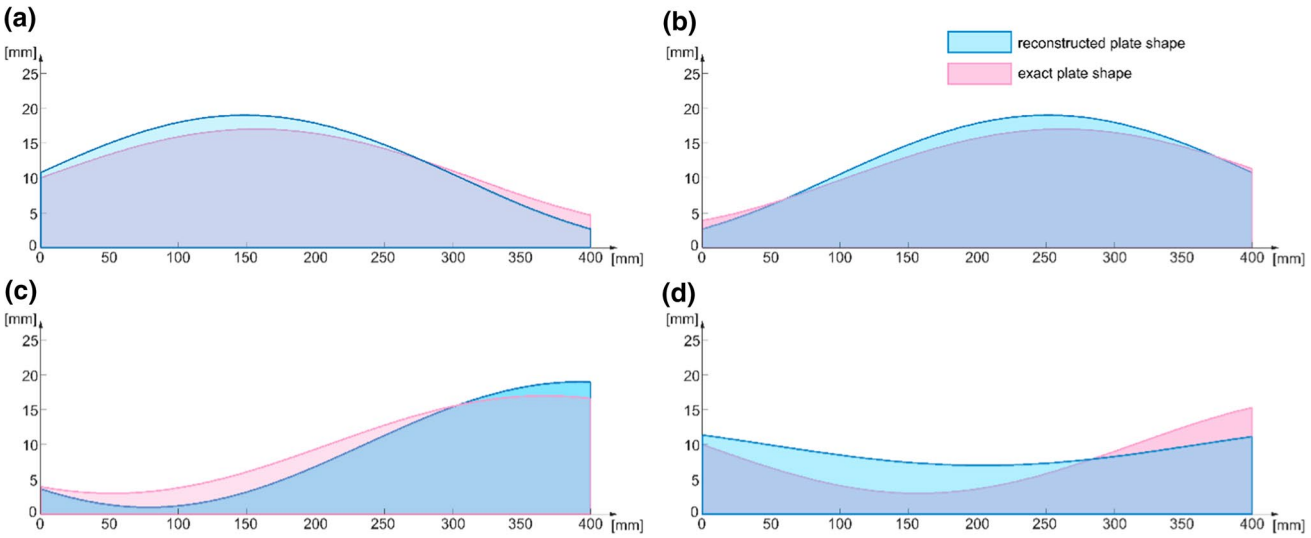

Fig. 16 Results of the II stage of the investigation aimed to determine the shape of the plate with non-constant thickness: the comparison of exact plate shapes with determined based on the experimental ToF measurements for **a** plate#1, **b** plate#2, **c** plate#3 and **d** plate#4

Table 4 Comparison of exact and experimentally determined amplitude and phase shift describing the sine-shaped plate surface

	Parameters defining sine function					
	A [mm]	A_e [mm]	$\Delta A = \lvert A - A_e \rvert$	φ	φ_e	$\Delta\varphi = \lvert\varphi - \varphi_e\rvert$
Plate #1	7	9	2	0	0.16π	0.16π
Plate #2	7	9	2	0.33π	0.3π	0.03π
Plate #3	7	9	2	0.67π	0.75π	0.08π
Plate #4	7	3	4	π	1.15π	0.15π

The comparison of extreme thicknesses indicates that in each considered case the highest inaccuracies were noted if the plate thickness was assumed to be constant (Table 5). Again the highest errors were highlighted with a grey colour. The maximum error was noted for plate #3 and was equal to over 700%. Moreover, the minimal thickness was overestimated. In the case of exact shape reconstruction, the maximum error was noted for plate #3 and was equal to 67%. This value cannot be considered low, but the value of $\Delta_a^{\min}$ calculated or average thickness was not lower than 148%, which means that taking into account the possibility of non-uniform thickness always resulted in more faithful results.

4.3.3 Stage III: plate shape determination for all parameters unknown

In the last stage, we assumed only the sine plate shape but the value of any parameter has not been established in advance. Despite that, the reconstructed plates coincide well with actual shapes (Fig. 17). For clarity, in Table 6 only the parameters obtained by solving the inverse problem and

Table 5 Comparison of the minimum and maximum thickness of experimentally reconstructed plate, average thickness determined based on the ToF with actual plate thickness

	Actual minimum thickness h_{min}	Actual maximum thickness h_{max}	$h^r_{\min}$ [mm]	$h^r_{\max}$ [mm]	$\Delta_r^{\min}$ [%]	$\Delta_r^{\max}$ [%]	h^e_a [mm]	$\Delta_a^{\min}$[%]	$\Delta_a^{\max}$[%]
Plate #1	4.702	17	2.70	19	42.60	11.76	11.70	148.81	31.17
Plate #2	3.938	17	2.70	19	31.44	11.76	13.10	232.66	22.94
Plate #3	3.000	17	1.00	19	66.67	11.76	24.10	703.33	41.76
Plate #4	3.000	15.3	7.00	11.4	133	25.49	5.60	370	63.39

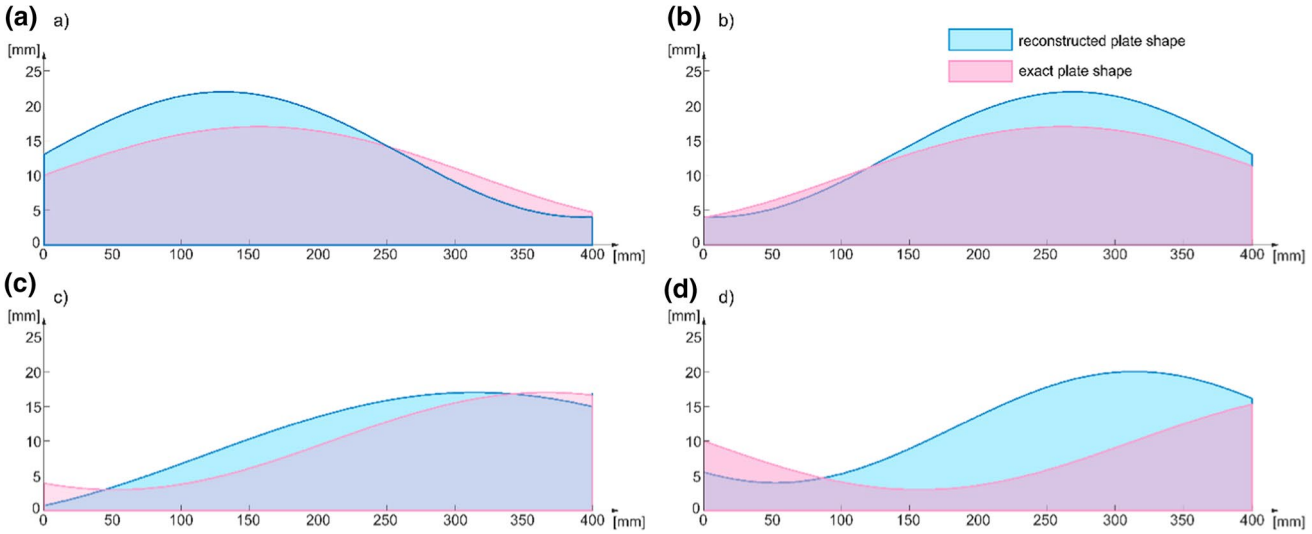

Fig. 17 Results of the III stage of the investigation aimed to determine the shape of the plate with non-constant thickness: the comparison of exact plate shapes with determined based on the experimental ToF measurements for **a** plate#1, **b** plate#2, **c** plate#3 and **d** plate#4

Table 6 Comparison of exact and experimentally determined parameters A, φ and k describing the sine surface of the plates (stage III)

	Parameters defining sine function							
	Amplitude [mm]		Phase shift		Wavenumber		Thickness [mm]	
	A_e	ΔA	φ_e	$\Delta\varphi$	k_e	Δk	h_e	Δh
Plate #1	9	2	0	0	12	2	13	3
Plate #2	9	2	0.528π	0.198π	10	0	13	3
Plate #3	9	2	0.303π	0.367π	8	2	8	2
Plate #4	8	1	0.528π	0.472π	12	2	12	2

the differences between calculated and exact parameters are presented. A particularly high agreement was obtained for plates #1 and #2. In both cases the amplitude was overestimated by 2 mm, the difference in phase shift does not exceed 0.03π, the wavenumber was overestimated by 2 or determined correctly, while the initial plate thickness was overestimated by 3 mm. In total, the reconstructed plates are characterized by a more convex shape than actual plates but it has not excluded the correct estimation of minimal plate thickness (Table 7).

5 Conclusions and discussion

In this study, the inherent dispersive properties of guided waves were used to determine the thickness variability of metallic plates. In the first stage of the investigation, the relationships between the ToF and thickness distribution of plate-like structures were derived and next were verified numerically and experimentally. The measurements were conducted on specially designed aluminum plates, which surfaces were defined by sine function varying in phase shift. Based on the presented results in this section, the important findings can be formulated.

First of all, the assumption about non-uniform plate thickness provided that extreme thicknesses extracted from reconstructed plate shape were much closer to actual extreme thicknesses than average thickness determined by dispersion curve fitting. The maximum relative error in the case of reconstructed shape was 67% and usually was significantly lower, while for dispersion curve-based average thicknesses the relative error reached over 700%.

The first stage of the study unambiguously proved that wave propagation velocity strongly depends on plate thickness distribution and the commonly applied assumption that based on the average velocity used to estimate the average thickness leads to significant inaccuracies resulting in both large over- and underestimation of the exact plate thickness. Rejecting the assumption about constant thickness led to much better results. In the majority of cases, an assumption about non-constant plate thickness leads to an overestimation of maximum thickness and underestimation of minimum thickness, while the assumption about uniform thickness results in the exact opposite situation, i.e., the critical minimum thickness determining the load capacity of the whole structure was overestimated.

Moreover, the proposed approach of searching for the optimal parameters defining the function describing plate shape does not require a greater number of measurements than the standard curve-based approach and the investigations were not preceded by reference measurements and the curve calibration.

Second, the number of assumed unknowns did not entail the deterioration of the quality of plate shape reconstruction. The inaccuracies summarized in Tables 3 and are similar (the maximum error is equal to 70–80%), while in the first case, two parameters (wavenumber and initial plate thickness) were known in advance. This is mainly because even an incorrect estimation of one of the searched parameters does not inextricably entail the deterioration of the reconstruction quality. The reconstructed shape presented in Fig. 17d does not coincide with the actual plate shape. However, it was still possible to determine the minimal and maximal plate thickness occurring along the propagation path. The only significant discrepancy is the location of the cross section with minimal thickness. Wrong estimation of any parameter describing plate surface excludes the possibility to indicate the position of the thinnest or the thickest place, even if the thickness has been estimated correctly.

Despite the promising results, the proposed approach is not without any limitations, which should be considered in future studies. It should be noted that in the majority of cases the amplitude of the reconstructed plate was overestimated. In both cases, numerical and experimental investigation the reconstructed amplitude was higher than the real amplitude. The similar errors in both cases suggest the presence of systematic error resulting from the selected method of ToF determination or/and the influence of edge reflections. The quality of shape reconstruction could be improved by the preceding choice of the favorable frequency range. Because the following study is the first step in the development shape reconstruction procedure based on the ToF measurements, the authors presented the results for the whole used frequency range. However, the analysis of the outcomes indicated that the lower frequencies (up to 160 kHz in this case) may be associated with greater inaccuracies caused by interference of S0 and A0 modes. For higher frequencies when A0 is faster than S0 the inaccuracies caused by waves overlapping were significantly lower.

Table 7 Comparison of the minimal thickness of the reconstructed plate and actual minimal plate thickness (stage III)

	Actual minimal thickness h_{min}	Actual maximum thickness h_{max}	Minimal thickness $h^r_{\min}$ (based on reconstructed shape)	Maximum thickness $h^r_{\max}$ [mm]	$\Delta_r^{\min}$ [%]	$\Delta_r^{\max}$ [%]
Plate #1	4.7024	17	4.000	22	14.94	29.41
Plate #2	3.9380	17	4.000	22	1.57	29.41
Plate #3	3.0000	17	0.669	17	77.93	0
Plate #4	3.0000	15.3	4.000	20	33.33	30.72

In both cases, the quality of reconstruction was the lowest for plate #4, which is also the only concave plate investigated here. The accuracy of shape reconstruction should be also considered in the context of the influence of plate shape and the possible evanescent modes. After reaching the thickness cutoff the adiabatic mode may reflect or convert into a different guided wave and thus, the concave shape and decreasing thickness of plate #4 might influence wave propagation phenomenon and registered signals.

In addition, in real cases, the function describing plate surface may be more complex and would demand expression as a sum of varying sinusoidal components, rather than being expressed by a single sine component. Thus, future studies should be focused on determining the parameters (amplitude, phase shift, initial thickness, and wavenumber) of the dominating components in the frequency spectrum of varying plate thickness. In addition, it should be taken into account that thickness variability may occur only in a certain range, not along the whole propagation path. It would demand considering the superposition of two cases: plate with constant and variable thickness.

Acknowledgements The first author greatly acknowledges the support of the Foundation for Polish Science (FNP).

Funding This research received no external funding.

Data availability Data will be made available on request.

Declarations

Conflict of interest The authors declare that they have no known competing financial interests or personal relationships that could have appeared to influence the work reported in this paper.

Ethical approval The authors state that the research was conducted according to ethical standards. This article does not contain any studies with human participants or animals performed by any of the authors.

References

1. Mitra M, Gopalakrishnan S. Guided wave based structural health monitoring: a review. Smart Mater Struct. 2021;25(5):27.
2. Bahador M, Zaimbashi A, Rahgozar R. Three-stage Lamb-wave-based damage localization algorithm in plate-like structures for structural health monitoring applications. Sig Proc. 2020;168: 107360.
3. Zima B. Damage detection in plates based on Lamb wavefront shape reconstruction. Measurement. 2021;117: 109206.
4. Lamb H. On waves in an elastic plate. Proc R Soc London Ser A. 1917;93:114–28.
5. Radzieński M, Doliński Ł, Krawczuk M, Palacz M. Damage localization in a stiffened plate structure using a propagating wave. Mech Syst Sig Pr. 2013;39:388–95.
6. Chen B-Q, Zhang X, Soares CG. The effect of general and localized corrosions on the collapse pressure of subsea pipelines. Ocean Eng. 2022;247:110719.
7. Maio L, Moll J, Memmolo V, Simon J. Ultrasonic inspection for ice accretion assessment: effects on direct wave propagation in composite media. Mech Syst Sig Pr. 2022;173: 109025.
8. Deng Q-T, Yang Z-C. Propagation of guided waves in bonded composite structures with tapered adhesive layer. Appl Math Modell. 2011;35:5369–81.
9. Moreau L, Minonzio JG, Talmant M, Laugier P. Measuring the wavenumber of guided modes in waveguides with linearly varying thickness. J Acoust Soc Am. 2014;135(5):2614–24.
10. Cho Y. Estimation of ultrasonic guided wave mode conversion in a plate with thickness variation. IEEE T Ultrason Fer. 2000;47(3):591.
11. Predoi MV, El-Kettani MEC, Hamitouche Z, Petre CC. Guided waves in plates with linear variation of thickness. J Acoust Soc Am. 2008;123(5):3834.
12. Marical P, El-Kettani MEC, Predoi MV. Guided waves in elastic plates with Gaussian section variation Experimental and numerical results. Ultrasonics. 2007;47:1–9.
13. Pagneux V, Maurel A. Lamb wave propagation in elastic waveguides with variable thickness. Proc R Soc London Ser A. 2006;462:1315–39.
14. Hu Z, An Z, Kong Y, Lian G, Wang X. The nonlinear S0 Lamb mode in a plate with a linearly-varying thickness. Ultrasonics. 2019;94:102–8.
15. Ech-Cherif M, El Kettani F, Luppé. A Guillet Guided waves in a plate with linearly varying thickness: experimental and numerical results. Ultrasonics. 2004;42:807–12.
16. Nurmalia N, Nakamura H, Ogi M, Hirao K. Nakahata, Mode conversion behavior of SH guided wave in a tapered plate. NDT E Int. 2021;45(1):156–61.
17. Moll J, Wandowski T, Malinowski P, Radzienski M, Opoka S, Ostachowicz W. Experimental analysis and prediction of antisymmetric wave motion in a tapered anisotropic waveguide. J Acoust Soc Am. 2015;138:299–306.
18. Moll J. Damage localization in composite structures with smoothly varying thickness based on the fundamental antisymmetric adiabatic wave mode. Ultrasonics. 2016;71:111–4.
19. Zima B, Woloszyk K, Garbatov Y. Corrosion degradation monitoring of ship stiffened plates using guided wave phase velocity and constrained convex optimization method. Ocean Eng. 2022;253: 111318.
20. Kabanikhin SI. Definitions and examples of inverse and ill-posed problems. J Inverse Ill Posed Probl. 2008;16:317–57.
21. Champeney DC. A Handbook of Fourier Theorems. University of East Anglia: Cambridge University Press; 1987.
22. Neuschwander K, Moll J, Memmolo V, Schmidt M, Bücker M. Simultaneous load and structural monitoring of a carbon fiber rudder stock: experimental results from a quasi-static tensile test. J Intell Mater Syst Struct. 2019;30:272–82.
23. Xu B, Yu L, Giurgiutiu V. Advanced methods for time-of-flight estimation with application to Lamb wave structural health monitoring, The 7th International Workshop on Structural Health Monitoring. Palo, Alto, CA: Stanford University; 2009.